Chromosome Res
https://doi.org/10.1007/s10577-022-09700-w

ORIGINAL ARTICLE

Alternative end-joining originates stable chromosome aberrations induced by etoposide during targeted inhibition of DNA-PKcs in ATM-deficient tumor cells

Marcelo de Campos Nebel · Micaela Palmitelli · Josefina Pérez Maturo · Marcela González-Cid

Received: 29 December 2021 / Revised: 29 April 2022 / Accepted: 9 May 2022

Abstract ATM and DNA-PKcs coordinate the DNA damage response at multiple levels following the exposure to chemotherapy. The Topoisomerase II poison etoposide (ETO) is an effective chemotherapeutic agent that induces DNA double-strand breaks (DSB), but it is responsible from the chromosomal rearrangements frequently found in therapy-related secondary tumors. Targeted inhibition of DNA-PKcs in ATM-defective tumors combined with radio- or chemotherapy has been proposed as relevant therapies. Here, we explored the DNA repair mechanisms and the genetic consequences of targeting the non-oncogenic addiction to DNA-PKcs of ATM-defective tumor cells after exposure to ETO. We demonstrated that chemical inhibition of DNA-PKcs followed by treatment with ETO resulted in the accumulation of chromatid breaks and decreased mitotic index in both A-T cells and ATM-knocked-down (ATM^{kd}) tumor cells. The HR repair process in DNA-PKcs-inhibited ATM^{kd} cells amplified the RAD51 foci number, with no correlated increase in sister chromatid exchanges. The analysis of post-mitotic DNA lesions presented an augmented number of persistent unresolved DSB, without alterations in the cell cycle progression. Long-term examination of chromosome aberrations revealed a strikingly high number of chromatid and chromosome exchanges. By using genetic and pharmacological abrogation of PARP-1, we demonstrated that alternative end-joining (alt-EJ) repair pathway is responsible for those chromosome abnormalities generated by limiting c-NHEJ activities during directed inhibition of DNA-PKcs in

Responsible Editor: Graham Dellaire and Beth Sullivan

Supplementary Information The online version contains supplementary material available at https://doi.org/10.1007/s10577-022-09700-w.

Marcelo de Campos Nebel and Micaela Palmitelli contributed equally to this work.

M. de Campos Nebel (✉) · M. Palmitelli · M. González-Cid
Laboratorio de Mutagénesis, Instituto de Medicina Experimental (IMEX), CONICET-Academia Nacional de Medicina, Buenos Aires, Argentina
e-mail: mnebel@hematologia.anm.edu.ar

J. Pérez Maturo
Programa de Medicina de Precisión Y Genómica Clínica, Facultad de Ciencias Biomédicas,, Instituto de Investigaciones en Medicina Traslacional, Universidad Austral-CONICET, Pilar, Argentina

J. Pérez Maturo
Consultorio Y Laboratorio de Neurogenética, Facultad de Medicina, Centro Universitario de Neurología "José María Ramos Mejía" Y División Neurología, Hospital J.M. Ramos Mejía, Universidad de Buenos Aires, Buenos Aires,, Argentina

Published online: 23 May 2022

ATM-deficient cells. Targeting the non-oncogenic addiction to DNA-PKcs of ATM-defective tumors stimulates the DSB repair by alt-EJ, which is liable for the origin of cells carrying stable chromosome aberrations that may eventually restrict the therapeutic strategy.

Keywords DNA and chromosome damages · double-strand break repair · cell cycle · etoposide · DNA-PKcs inhibition · ATM-deficient human cells

Abbreviations

Alt-EJ	Alternative end-joining
A-T	Ataxia-telangiectasia
ATM	Ataxia-telangiectasia mutated
ATMi	ATM inhibitor
ATR	Ataxia-telangiectasia and Rad3-related protein kinase
BN	Binucleated cells
BrdU	5-Bromo-2´-deoxyuridine
CENP-F	Centromere protein F
C-NHEJ	Classical non-homologous end-joining
DAPI	4,6-Diamidino-2-phenylindole
DMSO	Dimethylsulfoxide
DNA-PKcs	DNA-dependent protein kinase catalytic subunit
DNA-PKi	DNA-PKcs inhibitor
DSB	Double-strand breaks
ETO	Etoposide
FBS	Fetal bovine serum
γH2AX	Histone H2AX phosphorylated on serine 139
HR	Homologous recombination
Kd	Knockdown
Ku70/80	Heterodimeric protein
MI	Mitotic index
MRE11	Meiotic recombination 11 homolog A
NS	Non-silencing
PARP-1	Poly(APD-ribose) polymerse-1
PARP-1i	PARP-1 inhibitor
PBL	Peripheral blood lymphocytes
PBS	Phosphate buffered saline
PCR	Polymerase chain reaction
PFA	Paraformaldehyde
pGIPZ	Lentiviral vector
PI	Propidium iodide
PIKK	Phosphatidylinositol kinase-like kinase
qRT-PCR	Real-time quantitative reverse transcription PCR
RAD51	DNA repair protein RAD51 homolog 1
SCE	Sister chromatid exchanges
shRNAmir	Small-hairpin MicroRNA
Top2	Topoisomerase II

Introduction

The DNA damage response is a complex network designed to protect the cellular genome from damage through the activation of appropriate repair mechanisms, cell cycle checkpoints to provide time for repair and/or apoptosis for the removal of damaged cells from the population (Jeggo and Lobrich 2006). Central to this process is the phosphatidylinositol kinase-like kinase (PIKK), ataxia telangiectasia mutated (ATM), which phosphorylates different targets to affect cellular processes in response to DNA double-strand breaks (DSB) (Shiloh and Ziv 2013). These lesions are the most cytotoxic form of DNA damage, since they can lead to genome instability and chromosomal rearrangements, which are hallmarks of cancer cells (Alhmoud et al. 2020).

The enzyme Topoisomerase II (Top2) is the target of many important anti-cancer drugs including etoposide (ETO) (Zhang et al. 2021). The normal catalytic cycle of Top2 produces a transient enzyme-bridged DSB containing a covalent protein-DNA reaction intermediate, where Top2 remains attached to DNA via a 5´tyrosyl phosphodiester linkage. ETO stabilizes this intermediate resulting in permanent DSB that can lead to cell death. Thus, drugs that stabilize the Top2-DNA complexes are referred to as Top2 poisons (Nitiss 2009).

There are two major DSB repair pathways and several back-up pathways that promote rejoining at the cost of lowered fidelity (Ranjha et al. 2018). The main pathways include a potentially error-prone classical non-homologous end joining (c-NHEJ) mechanism in which two broken ends are able to be joined; and an error-free homologous recombination (HR) process involving extensive resection and utilizing an intact copy of the damaged locus. Alternative end-joining (alt-EJ) is a back-up pathway, which utilizes microhomology sequences close to strand breaks to carry out DSB repair with single strand break repair proteins. However, not all alt-EJ events involve microhomology sequences (Seol et al. 2018).

During c-NHEJ, DNA ends are recognized by the Ku70/80 heterodimer, which requires the activation of the PIKK, DNA-dependent protein kinase catalytic subunit (DNA-PKcs) for promoting end processing and then ligation by XRCC4/Ligase4 complex. On the other hand, poly(ADP-ribose) polymerase-1 (PARP-1) is a protein implicated in alt-EJ, whose DNA end binding affinity allows to exert an inefficient competition with Ku, to switch end joining pathway from c-NHEJ to alt-EJ. Genetic and biochemical studies implicate Ligase1 and Ligase3 in the final ligation step of alt-EJ (Caracciolo et al. 2021).

In spite of its ability for removing DSB, alt-EJ pathway often commits severe DSB processing errors, resulting in large alterations at the junctions and the formation of chromosomal translocations (Iliakis et al. 2015). These types of structural chromosome aberrations are clinically relevant as they are associated with numerous human cancers (Roukos and Misteli 2014). In this sense, the use of the Top2 poison ETO is related to the development of therapy-related secondary leukemia, especially acute myeloid leukemia that shows chromosome rearrangements, frequently translocations involving band 11q23 (Zhang et al. 2021).

ATM-deficient tumors are frequently associated to chemotherapy resistance (Austen et al. 2007; Jiang et al. 2009). Thus, improvements to those therapies must be considered. In this regard, a synthetic lethality effect between ATM and DNA-PKcs has been reported (Riabinska et al. 2013), which open the therapeutic strategy for several ATM-defective solid and hematologic tumors.

Here, we analyzed the chromosome damage induced by the Top2 poison ETO in G2-phase on ATM-deficient human cells during the non-oncogenic addiction to DNA-PKcs in order to determine the involvement of DNA repair mechanisms in the genesis and progression of chromosome aberrations, which may affect the therapeutic strategy outcome.

Materials and Methods

Human cell cultures, gene knockdown and drug treatments

The human HeLa cell line was kindly provided by Dr. M.C. Carreras, INIGEM-UBA, Hospital de Clínicas José de San Martín, Buenos Aires, Argentina. Cells were grown in RPMI 1640 medium (Gibco, #22,400–89) supplemented with 10% fetal bovine serum (FBS, Biotecnológico, Internegocios SA) and antibiotics (Gibco, #15,240–062). Cultures were maintained at 37ºC in a humidified atmosphere of 5% CO2 in air. HeLa cells were transfected with pGIPZ human shATM (Open Biosystems, clone id: V2LHS_348), pGIPZ human shPARP-1 (Open Biosystems, clone id: V2LHS_201984) or pGIPZ non-silencing (NS) shRNA control (OpenBiosystems, #RHS4346) using Lipofectamine 2000 (Invitrogen, #11,668–019) according to manufacturer's instructions. After 48 h, the cells were grown in selection medium containing puromycin 1 µg/ml (Invivogen, #ant-pr-1) which was renewed every third day. The selection process was performed by 3–4 weeks and clonal selection of stable transfectants was carried out. The levels of knockdown were monitored by qRT-PCR, and HeLa ATM^{kd} cells were also confirmed by western blot. The knockdown cell lines generated were routinely tested by PCR for mycoplasma. Additionally, heparinized peripheral blood lymphocytes (PBL) were obtained by venipuncture from a 21-year-old ataxia-telangiectasia patient (The A-T patient provided written consent, Institutional Ethics Committee, Hospital J. M. Ramos Mejia, Buenos Aires, Argentina) (Perez Maturo et al. 2020) and a 27-year-old healthy non-smoking donor free of any known exposure to genotoxic agents. For each culture, 450 µl of PBL was cultured in 4.5 ml of RPMI 1640 medium with 15% FBS, antibiotics and 2% phytohemagglutinin M (Gibco, #10,576–015). Cultures were incubated at 37 °C for 72 h. ETO (Sigma-Aldrich, E1383), NU7026 (Calbiochem, #260,961, DNA-PKi), BYK204165 (Santa Cruz Biotechnology, #sc-214642, PARP-1i) and KU55933 (Calbiochem, #118,500, ATMi) were dissolved in DMSO. HeLa ATM^{kd}, HeLa PARP-1^{kd}, HeLa NS cells and PBL were exposed to DMSO 0.5%, DNA-PKi 10 µM, PARP-1i 1 µM or 10 µM or ATMi 10 µM, and ETO at different concentrations and by different periods of time for respective assays.

γH2AX detection in G2 phase by flow cytometer

HeLa ATM^{kd} and NS cells were treated with DMSO for 2 h, DNA-PKi for 3 h, ETO 2 µg/ml for 2 h or

a combination of both drugs (pre-treated with DNA-PKi for 1 h prior to ETO treatment for 2 h). After washing twice in PBS, cells were fixed in 90% methanol for at least 1 h at -20 °C. Cells were immunostained with antiγH2AX antibody (1:200, Millipore clone JBW301) followed by Alexa Fluor 488-conjugated secondary antibody (1:250, Invitrogen, #A-11001). RNAse A treatment (200 µg/ml, Biodynamics, #B181-1) was performed and then counterstaining with propidium iodide (PI, 10 µg/ml, Becton–Dickinson, BDB-556463). Acquisition of 20,000 cells/sample was carried out using a FACSCalibur flow cytometer (Becton–Dickinson) using the Cell Quest software. Appropriate isotype controls were added and the percentage of γH2AX + cells in G2 phase was determined in four independent experiments.

Structural chromosome alterations and mitotic index (MI) in HeLa and human lymphocyte cells

HeLa ATM^{kd} and NS cells were treated with DMSO for 2 h, DNA-PKi until the end of the experiment, ETO 2 µg/ml for 1 h or a combination of both drugs DNA-PKi/ETO (pre-treated with DNA-PKi for 1 h followed by ETO for 1 h), and incubated for 6 h to reach the immediate metaphase. Human PBL were treated at 36 h with DMSO, DNA-PKi, and ETO 0.25, 0.5 or 1.0 µg/ml or a combination of DNA-PKi/ETO during the last 36 h of cultures. Colcemid (Gibco, #15,212–012) 0.1 µg/ml was added 90 min before harvesting; cells were exposed to hypotonic solution KCl 0.075 M, fixed in methanol: glacial acetic acid (3:1) and stained with Giemsa (Merck, AR11092041022) 10% for 2.5 min. In HeLa ATM^{kd} and NS cells, chromatid breaks and exchanges were analyzed in 50 metaphases/treatment in three independent experiments. For the MI analysis, cells were fixed with 2% paraformaldehyde (PFA) and permeabilized with 100% methanol. Cells were immunostained with anti-phosphoSer10-histone H3 antibody (1:50, Santa Cruz Biotechnology, sc8656-R) followed by DyLight 488-conjugated secondary antibody (1:250, Thermo Scientific). RNAse A treatment and PI counterstaining was performed, and 30,000 cells were analyzed in three independent experiments by flow cytometry. In PBL, chromatid breaks and exchanges were analyzed, when it was possible, in 50 metaphases and the MI was evaluated in 1,000 interphase nuclei and expressed in percentages. Two independent experiments were performed.

RAD51 immunofluorescence and sister chromatid exchanges (SCE)

For the evaluation of RAD51 foci formation, HeLa ATM^{kd} and NS cells were grown on coverslips, treated as previously described and incubated for 5–6 h. Cells were then fixed with 2% PFA and permeabilized with 0.25% Triton X-100 in PBS. Immunofluorescence was performed using primary antibodies against CENP-F (1:200; Thermo Scientific, MA1-3,160,023,185) and RAD51 (1:250, Santa Cruz Biotechnology, sc-8349) followed by exposure to Alexa Fluor 488- anti-mouse (1:250, Invitrogen, #A-11001) and Alexa Fluor 594- anti-rabbit conjugated secondary antibodies (1:200, Thermo Scientific, A11072), respectively. DNA was stained with 4,6-diamidino-2-phenylindole (DAPI, Vector Laboratories). The number of RAD51 foci/nucleus was analyzed by visual scoring in 100 CENP-F + cells in two independent experiments.

For the SCE analysis, cells were incubated in the presence of 10 µg/ml 5-bromo-2´-deoxyuridine (BrdU, Sigma-Aldrich, #B-5002) for 44 h (about two rounds of replication), treated with ETO 1.5 µg/ml and incubated for 6 h. Cells were exposed to colcemid, hypotonic solution and fixed. Air-dried chromosome preparations were made and a modification of the fluorescence-plus-Giemsa method was applied to obtain harlequin chromosomes. The average frequency of SCE/chromosome was determined from the analysis of 100 metaphases in three independent experiments.

γH2AX and MRE11 foci analysis in the main nucleus of binucleated (BN) cells

HeLa ATM^{kd} and NS cells were seeded on coverslips, treated with DMSO for 2 h, DNA-PKi until the end of the experiment, ETO 2 µg/ml for 1 h or a combination of both drugs, and incubated for 11 h to reach the following cell cycle. Cytochalasin B (Calbiochem, cat# 250,233) 3 µg/ml was added during the last 4 h before harvesting; cells were exposed to

hypotonic solution for 8 min and fixed with 2% PFA and permeabilized with 0.25% Triton X-100. Immunofluorescence was carried out using a primary antibody against γH2AX (1:500). For MRE11 detection, cells were pre-extracted with 0.5% Triton X-100 in PBS for 2.5 min before fixation and permeabilization. MRE11 foci were detected with a primary antibody against MRE11 (1:500, Cell Signaling, #31H4). In both cases, appropriate Alexa Fluor 594-conjugated secondary antibodies (1:300) were utilized and DNA counterstained with DAPI. Five hundred BN cells were counted for each treatment and cells containing γH2AX foci or ≥ 5 foci of MRE11/nucleus were scored as positive. The percentage of BN cells was scored in 1,000 cells for each treatment. In each case, three independent experiments have been performed.

Cell cycle assessment

HeLa ATM^{kd} and NS cells were cultured as described above. After 8, 16 and 40 h of incubation, attached and unattached cells were collected and fixed with 90% methanol. RNAse A treatment and PI counterstaining was performed. Acquisition of 20,000 cells/sample was done using a FACSCalibur flow cytometer. The phases of cell cycle were analyzed using FCS Express 4 software. Three independent experiments have been evaluated.

Dicentric chromosomes in metaphase following c-NHEJ or alt-EJ inhibition

HeLa ATM^{kd} and NS cells were treated with DMSO for 2 h, DNA-PKi or PARP-1i 10 μM or combined DNA-PKi/PARP-1i until the end of the experiment and ETO 2 μg/ml for 1 h in the presence or absence of the inhibitors, and incubated for 26 h adding BrdU during the last 8 h to detect the second mitosis. Metaphase chromosomes were obtained as described above. Subsequently, slides were incubated in blocking solution containing primary antibody against BrdU (1:100, Becton–Dickinson, B44) for 1 h, followed by exposure to Alexa Fluor 488- anti-Mouse conjugated secondary antibody (1:300), and DNA was stained with DAPI. The frequency of dicentric chromosome was evaluated in 150 BrdU + cells per treatment in three independent experiments.

Structural chromosome aberrations in HeLa ATM^{kd} and PARP-1^{kd} cells

HeLa ATM^{kd} and NS cells were treated as previously described, and incubated for 6 days (144 h). Also, HeLa PARP-1^{kd} and NS cells were treated with DMSO for 2 h, ATMi until the end of the experiment, ETO 2 μg/ml for 1 h or a combination of both drugs ATMi/ETO and incubated for 6 days (144 h). For each treatment, at least 150 metaphases were analyzed for the induction of chromatid and chromosome breaks and exchanges in three independent experiments.

Clonogenic survival assay

HeLa ATM^{kd} (6×10^3) and NS (8×10^2) cells were seeded and pre-treated or not with DNA-PKi 10 μM or PARP-1i 1 μM for 2 h, prior to treatment with different concentrations of ETO (0.05, 0.1, 0.5 and 1.0 μg/ml) for 16 h. The cells were washed with PBS and cultured in fresh complete media for 14 days. Then, cells were rinsed with PBS, fixed with 100% methanol, and stained with 1% crystal violet. Colonies containing more than 50 cells were scored. Survival fraction was estimated as the ratio of colonies in treated cultures compared with control cultures and expressed in percentages in three independent experiments.

Statistical analysis

Statistical analysis were performed using GraphPad Prism 8.0 software (GraphPad Software Inc., USA). Data were presented as means ± sem and they were analyzed with a two-tailed Student's *t* test, except for RAD51 foci, which was evaluated with the nonparametric two-tailed Mann–Whitney *U* test. Statistical significance was considered at $p < 0.05$.

Results

ETO-induced DNA damage in ATM- and DNA-PKcs-deficient human cells

Following the selection of stably transfected HeLa cells with a specific shRNAmir sequence against ATM, the expression of ATM in different cellular clones was evaluated. The shATM#1 showed the lowest ATM expression level (Supplementary Fig. S1a and S1b, hereafter referred to as HeLa ATM^{kd}) and was used throughout the different experiments.

One of the earliest responses to DNA damage is the phosphorylation of a highly conserved histone variant, H2AX, yielding a modified form called γH2AX (Kopp et al. 2019). ETO and DNA-PKi/ETO treatments induced a significant and similar increase ($p < 0.005$) in the percentage of γH2AX-positive cells in the G2 phase of HeLa ATM^{kd} and NS cells when immediately evaluated by flow cytometry (Fig. 1a). Since the Top2α activity increases throughout the cell cycle, the different treatments were carried out in G2 phase, where its maximal activity is almost reached (Meyer et al. 1997). Furthermore, all DSB repair mechanisms operate in this phase (Mladenov et al. 2016).

DSB are considered the critical primary lesion in the formation of chromosomal aberrations (Obe and Durante 2010). Chromosome analysis at the first metaphase following G2 phase treatments revealed that ETO led to an important increase in chromatid type aberrations, breaks and exchanges, relative to levels found in untreated control and DMSO- or DNA-PKi-treated cells in both HeLa cell lines (Fig. 1b-c). In the presence of DNA-PKi/ETO, an increased frequency of chromatid breaks and exchanges was also observed, although this increase was statistically significant in the case of chromatid breaks in ATM^{kd} cells compared to NS cells (6.8 ± 0.7 vs. 4.3 ± 0.07, $p = 0.0195$). In addition, mitotic cells were scored as phosphoH3-positive cells by flow cytometry in both cell lines. At 6 h after treatments, we noted a pronounced decline in MI of DNA-PKi/ETO treatment with respect to ETO alone, being this reduction larger in ATM-deficient cells (Fig. 1d). ATM-deficient cells usually show an impaired S-phase and early G2 checkpoints [Xu et al. 2002]. Strikingly, ETO-treated ATM^{kd} cells showed a low MI compared to NS cells. Thus, we performed a checkpoint assay at short times (Supplementary Fig. S2). We determined that in response to ETO, NS cells rapidly activated early G2 checkpoint, which was absent in ATM^{kd} cells. However, ETO-treated ATM^{kd} cells showed a decreased mitotic ratio compared to NS at 3 h post-treatment, resulting in an ATM-independent accumulation of cells in G2.

To confirm the chromosomal damage obtained in HeLa ATM^{kd} cells on non-tumoral cells, we examined human lymphocytes from an A-T patient and a normal donor (Fig. 1e-g). Overall, A-T PBL exhibited an important increase in the frequency of chromatid breaks and exchanges respect to normal PBL, being statistically significant ($p < 0.0001$) in the case of chromatid breaks treated with ETO 0.5 μg/m in the presence or not of DNA-PKcs inhibitor (Fig. 1e and Supplementary Fig. S3). Only a few metaphases were obtained with this concentration of ETO in the presence or not of the DNA-PKi. In parallel, a marked decrease in the MI was also observed in A-T patient (Fig. 1g, $p < 0.0002$).

These results suggest that lack of ATM together with the chemical inhibition of DNA-PKcs caused an accumulation of ETO-induced DSB, an increase of chromatid breaks and a reduction of mitosis cells, consistent with the role of ATM and c-NHEJ in the maintenance of genome integrity.

DNA-PKcs and ATM regulate the initial steps of ETO-induced HR repair of DSB

To assess the effect of DNA-PKcs and ATM on HR, we analyzed RAD51 foci formation and SCE at 6 h post-treatment (Fig. 2). The number of RAD51 foci/nucleus was similarly increased after ETO treatment in NS cells pretreated with DNA-PKi (9.6 ± 0.6) and in ATM^{kd} (9.9 ± 0.7) cells (Fig. 2a). In addition, RAD51 foci signals were significantly enhanced by the DNA-PKi in ATM^{kd} (12.9 ± 0.8, $p < 0.0001$). Then, RAD51 is dissociated from the ends of DNA to allow DNA synthesis and resolution. HR is the principal mechanisms responsible for SCE in vertebrate cells (Sonoda et al. 1999). For SCE analysis in ATM^{kd} cells, the BrdU incorporation during two rounds of replication and the treatment with ETO 2 μg/ml resulted in an important reduction of assessable metaphase. Thus, both cell lines were exposed to a lower concentration of ETO (1.5 μg/ml). We found that values of SCE/chromosome in DMSO,

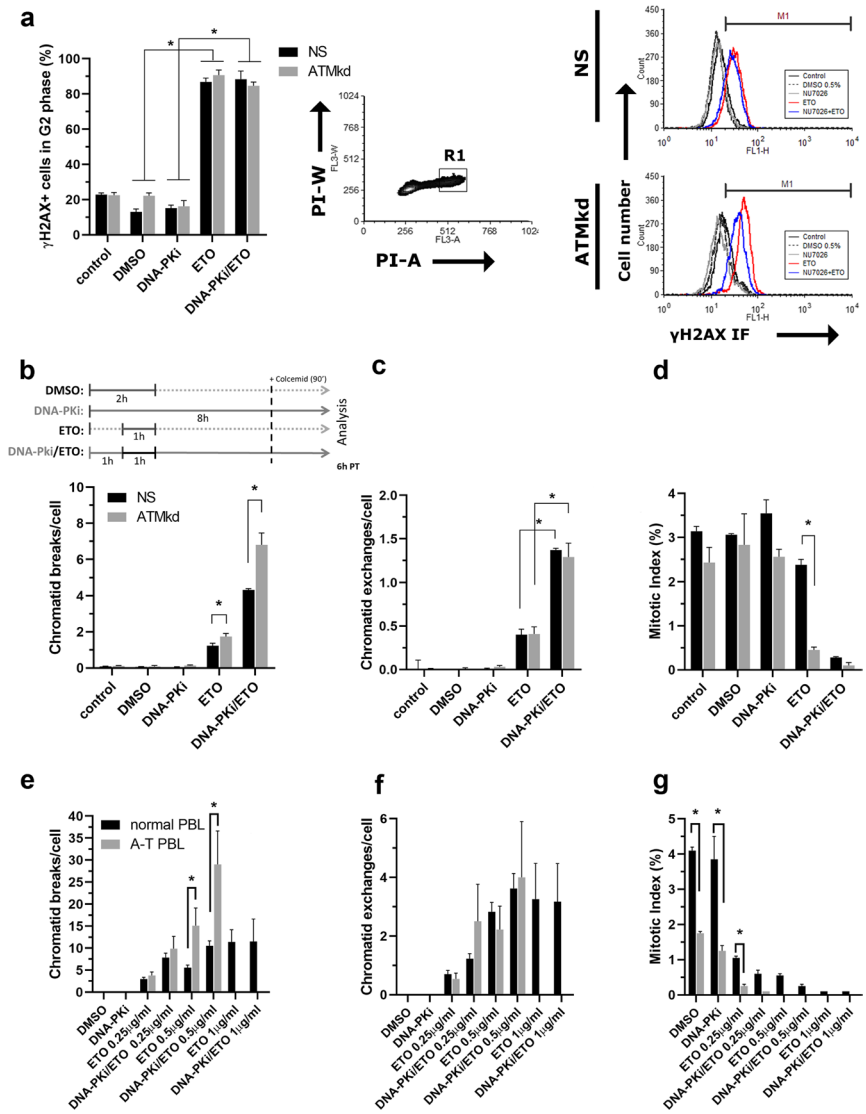

Fig. 1 Increased ETO-induced DNA damage following DNA-PKcs inhibition in ATM-defective human cells. **a**. γH2AX positive HeLa NS and HeLa ATM^{kd} cells were treated in G2 phase and analyzed immediately by flow cytometry. *Left panel:* Bar graph showing the percentage of G2 γH2AX + cells, $*p < 0.005$. *Middle panel:* Representative density plot showing the G2 population (R1) selected for the analysis. PI-A = propidium iodide area (FL3-A), PI-W = propidium iodide weight (FL3-W). *Right panel:* Representative histogram plots showing the R1 population analyzed for γH2AX intensity of fluorescence (γH2AX IF). M1 = marker (γH2AX + cells). **b** and **c.** Structural chromosome aberrations evaluated in HeLa NS and ATM^{kd} cells at 6 h post-treatment (PT) with ETO 2 μg/ml for 1 h and pre-treated or not with the DNA-PKcs inhibitor (DNA-PKi, NU7026) 10 μM by 1 h. **b.** *Upper panel:* Schematic representation of treatments (b-d) over the time until the analysis. *Lower panel:* Chromatid break frequencies, $*p < 0.021$. **c**. Chromatid exchange frequencies, $*p < 0.0001$. **d**. Mitotic index analysis in cells immunostained with anti-pSer10-H3 antibody assessed by flow cytometry, $*p = 0.0002$. **e** and **f**. Structural chromosome aberrations in human peripheral blood lymphocytes (PBL) of normal donor and A-T patient. PBL were pretreated or not with DNA-PKcs inhibitor NU7026 10 μM for 1 h and treated with different concentrations of ETO during the last 36 h of cultures. **e.** Chromatid breaks per cell evaluated in the first metaphase, $*p < 0.0001$. **f.** Chromatid exchanges per cell evaluated at first metaphase. **g.** Mitotic index analysis in 1,000 interphase nuclei per treatment, $*p < 0.0002$

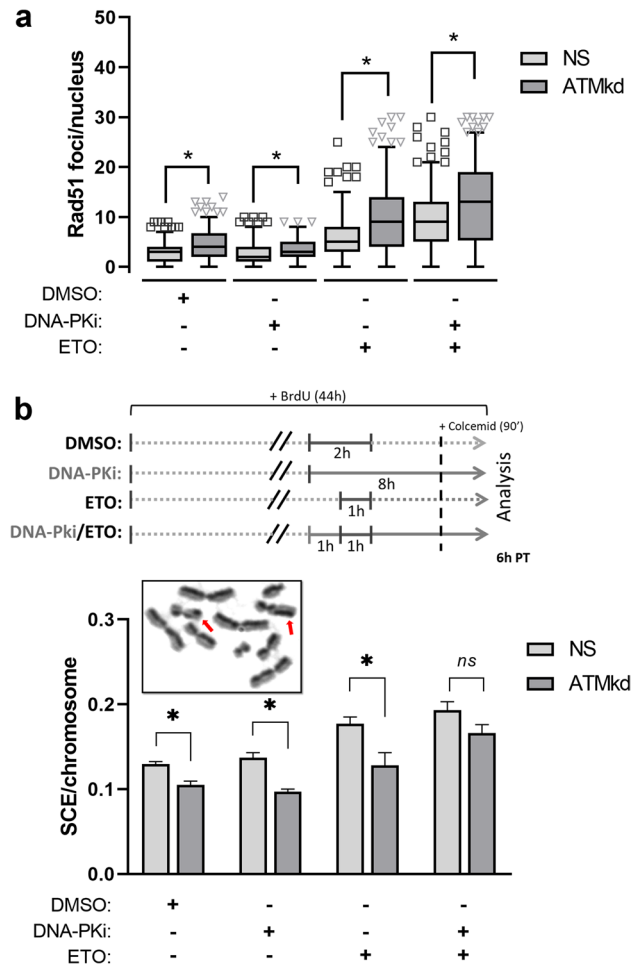

Fig. 2 HR repair of ETO-induced DSB in an ATM- and DNA-PKcs-deficient context. **a**. Rad51 foci per nucleus in CENP-F + HeLa NS and HeLa ATM^{kd} cells. Cells were pre-treated or not with DNA-PKcs inhibitor (DNA-PKi, NU7026) for 1 h and treated with ETO 2 µg/ml by 1 h, $*p < 0.0001$. **b**. *Upper panel:* Schematic representation of treatments over the time until the analysis. *Lower panel:* Sister chromatid exchanges (SCE) per chromosome were analyzed in HeLa NS and HeLa ATM^{kd} cells at 6 h post-treatment (PT). $*p < 0.0025$. *Inside image:* Harlequin-like chromosomes. Red arrows: chromosomes with sister chromatid exchanges

DNA-PKi and ETO-treated ATM^{kd} cells were significantly lower than that observed in NS. Although DNA-PKi/ETO treatment induced an increase in both cell lines, it was higher in HeLa ATMkd (Fig. 2b), making the statistical differences between both cell lines disappear. These findings indicate that a combined depletion of ATM and DNA-PKcs activities amplified notoriously the HR-mediated RAD51 foci formation of cells exposed to ETO, which was not reflected in the SCE levels, suggesting that the formation of long patches exchanges was not substantially affected.

ETO-induced DSB progress to post-mitotic G1 cells in a DNA-PKcs and ATM deficient context

The role of DNA-PKcs and ATM in the progression of DNA damage was assessed by the presence of γH2AX foci in the main nuclei of post-mitotic G1 phase cells (Fig. 3c). Figures 3a and 3b show the percentage of BN cells in different categories based on the number of γH2AX signals in the main nuclei of NS and ATM^{kd} cells, respectively. It was observed in ATM^{kd} cells an increased basal DNA damage in DMSO- or DNA-PKi-treated cells, compared to NS cells. Deckbar et al. (Deckbar et al. 2007) reported that immortalized human fibroblasts were released from the G2/M checkpoint with ~ 20 γH2AX foci after X-irradiation. Therefore, we estimated the percentage of BN cells with ≥ 21 γH2AX foci in ETO- and DNA-PKi/ETO-treated cells. These results revealed that the percentage of BN cells with ≥ 21 γH2AX foci in the main nuclei was 21.7 ± 2.7% in NS cells treated with DNA-PKi/ETO, while in ATM^{kd} cells treated with ETO alone, this percentage was 26.8 ± 1.5%. Lastly, in ATM^{kd} treated with the combination, this

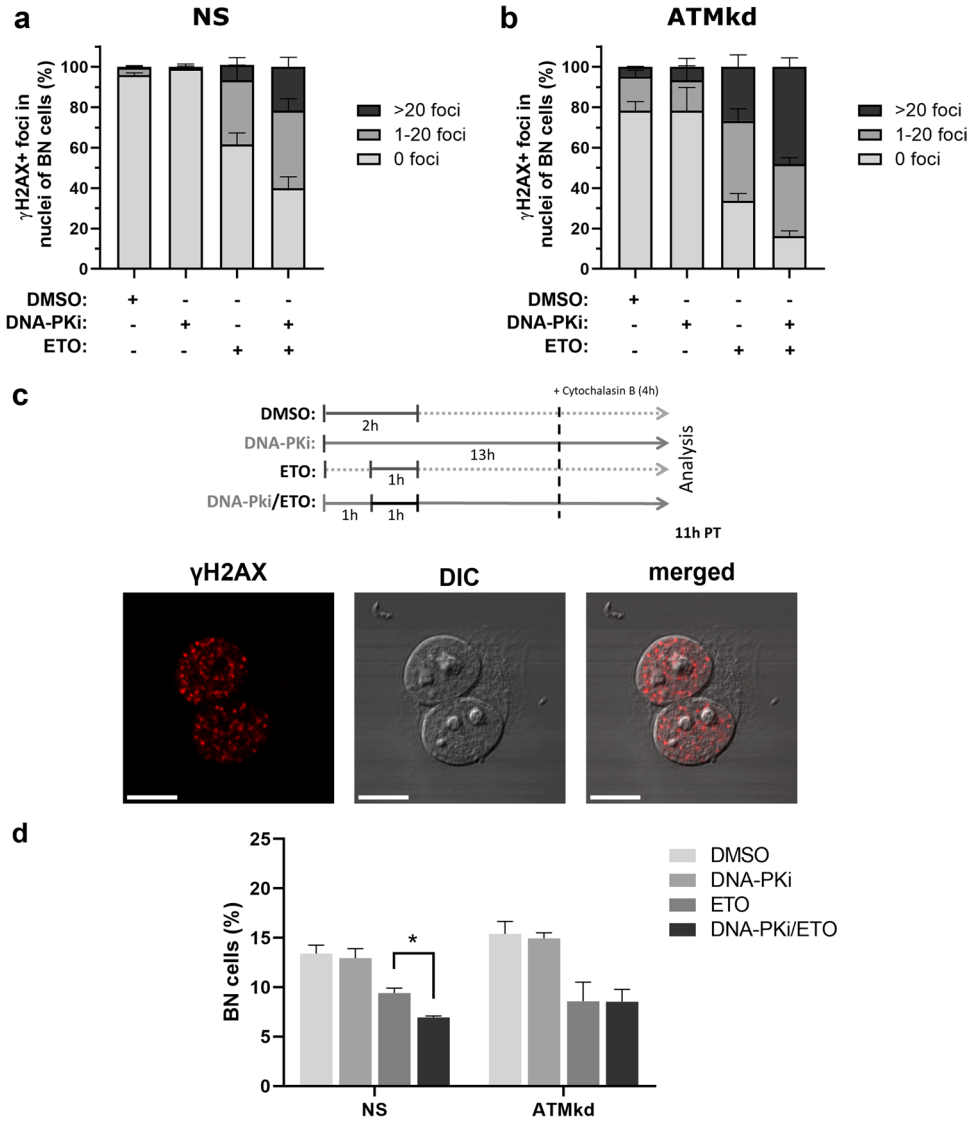

Fig. 3 Progression of DNA DSB induced by ETO in G2 after DNA-PKcs inhibition in HeLa NS and HeLa ATM^{kd} cells. γH2AX foci were analyzed in post-mitotic G1 binucleated (BN) cells at 11 h post-treatment (PT). **a.** Distribution of γH2AX foci number in the main nuclei of HeLa NS BN cells. **b.** Distribution of γH2AX foci number in the main nuclei of HeLa ATM^{kd} BN cells. **c.** *Upper panel:* Schematic representation of treatments over the time for the analysis of BN cells. *Lower panel:* Representative images of a BN cell harboring γH2AX foci. Scale bar = 8 μm. DIC = differential interference contrast. **d.** Percentage of BN cells. *$p = 0.0049$

percentage raised to $48.2 \pm 2\%$ ($p = 0.0002$ vs. NS cells treated with DNA-PKi/ETO and $p = 0.0004$ vs. ATM^{kd} cells treated with ETO). Therefore, the lack of both ATM and DNA-PKcs caused an additive increase in the percentage of BN cells with DSB, relative to the defect in each individual factor. In addition, we evaluated the percentage of BN cells after the different treatments (Fig. 3d). In HeLa NS cells, the combined treatment significantly reduced the percentage of BN cells, in relation to ETO treatment alone ($7.0 \pm 0.2\%$ vs. $9.4 \pm 0.5\%$, $p = 0.0049$). Regarding ATM^{kd} cells, no differences between both treatments were observed, being $8.6 \pm 1.9\%$ in ETO-treated cells and $8.5 \pm 1.3\%$ in DNA-PKi/ETO-treated cells.

Further, we scored the MRE11 (meiotic recombination 11) and γH2AX foci formation on parallel

samples in post-mitotic G1 cells (Supplementary Fig. S4). MRN (MRE11, RAD50 and NBS1) complex is a sensor of DSB that controls the DNA damage response by ATM and regulates DSB repair. MRE11 activity initiates DNA end resection, which was reported to be required to remove Top2-DNA complexes from DSB ends (Lee et al. 2012). A good correlation between the increased percentages of MRE11-positive BN cells and those γH2AX-positive BN cells during different treatments in both cell lines was found (NS cells, $r=0.945$ and $p=0.015$; ATM^{kd} cells, $r=0.958$ and $p=0.010$). Nevertheless, ATM-deficient cells combined with the DNA-PKi/ETO treatment, showed an increase in the percentage of γH2AX-positive BN cells ($83.6\pm2.4\%$, $p=0.0002$) compared to those MRE11-positive ones ($63.0\pm6.6\%$; Supplementary Fig. S4b). On the other hand, ATM cells displayed a higher fraction of γH2AX and MRE11-labeled cells than NS. Our data support a direct association between DSB and the Mre11-mediated DNA-end resection in G1 phase BN cells. Taken together, the chemical inhibition of DNA-PKcs in ATM-deficient cells led to persistent unresolved DSB in post-mitotic BN cells.

DNA-PK inhibition does not affect the cell cycle progression of ATM deficient cells treated with ETO.

DNA damage triggers the activation of checkpoint pathways that transiently delay or arrest cell cycle progression to facilitate repair. The cell cycle distribution of HeLa NS and ATM^{kd} cells in the presence of ETO and DNA-PKi at 8, 16 and 40 h post-treatment was evaluated. It was established that HeLa cells express defects in p53 signaling (Del Nagro et al. 2014) with a lack of a G1 arrest after DNA damage.

As shown in Figs. 4a and 4c, there were increased proportions of NS cells at G2/M phase at 8 h, as demonstrated by a 4.2–4.5-fold increase of the percentage of G2/M cells in ETO- and DNA-PKi/ETO-treated cells, respectively, relative to their respective controls. However, as depicted in Figs. 4b and 4d, there was a lower proportion of G2/M ATM^{kd} cells at 8 h, where the percentage of cells were increased by 2.3–2.5-fold in ETO and DNA-PKi/ETO respect to the percentage found in DMSO- or DNA-PKi-treated cells, respectively. At 16 h the G2/M fraction of ETO- and DNA-PKi/ETO treated NS cells dropped down to 2.3–2.1-fold relative to their controls, respectively (Fig. 4c). No further differences were found for ETO and DNA-PKi/ETO treatments in NS cells at 40 h with G2/M levels being from 1.7–1.4-fold, respectively, to their controls. Conversely, ETO- and DNA-PKi/ETO treatments in ATM^{kd} cells showed at 16 h G2/M fractions that were similar to those found at 8 h (Fig. 4d), with levels relative to controls that were 2.2–2.3-fold increased. By 40 h, ETO- and DNA-PKi/ETO treated ATM^{kd} cells showed G2/M fractions that were 1.5–1.8-fold their respective controls.

In conclusion, DNA-PKi did not alter significantly the progression of the cell cycle of ETO-treated ATM^{kd} cells harboring unrepaired DNA damage.

Long-term chromosome rearrangements induced by ETO in ATM and DNA-PKcs deficient cells are mediated by an alt-EJ repair process

The disruption of ATM (Bennardo and Stark 2010) or DNA-PKcs (Gunn et al. 2011) led to a higher usage of incorrect DNA ends, favoring chromosome rearrangements. At 26 h post-treatment, we evaluated dicentric chromosomes at second metaphase in HeLa NS and ATM^{kd} cells pre-treated with DNA-PK, PARP-1 or DNA-PK/PARP-1 inhibitors in combination with ETO. To detect the second metaphases, BrdU was incorporated for 8 h prior to preparation of chromosome spreads (Fig. 5a). In these metaphases in the absence of ATM and DNA-PKcs, the values of dicentric chromosomes in BrdU-positive cells were similar in HeLa NS treated with DNA-PKi/ETO (0.31 ± 0.09) and HeLa ATM^{kd} treated with ETO alone (0.29 ± 0.05). Likewise, the combined treatment caused a synergistic increase in the frequency of dicentric chromosomes in ATM^{kd} cells (0.89 ± 0.08, $p<0.0001$) compared to NS cells. Thus, we considered that such increment in dicentric chromosomes in ATM and DNA-PKcs-deficient cells could reflect the contribution of alt-EJ pathway in the DSB repair. To test this hypothesis, we treated NS and ATM^{kd} cells with BYK204165, a chemical inhibitor of PARP-1 (PARP-1i), since this protein has a fundamental role in alt-EJ. The results denoted an important reduction in dicentric chromosomes in HeLa ATM^{kd} cells treated with PARP-1i/ETO (0.13 ± 0.04) or

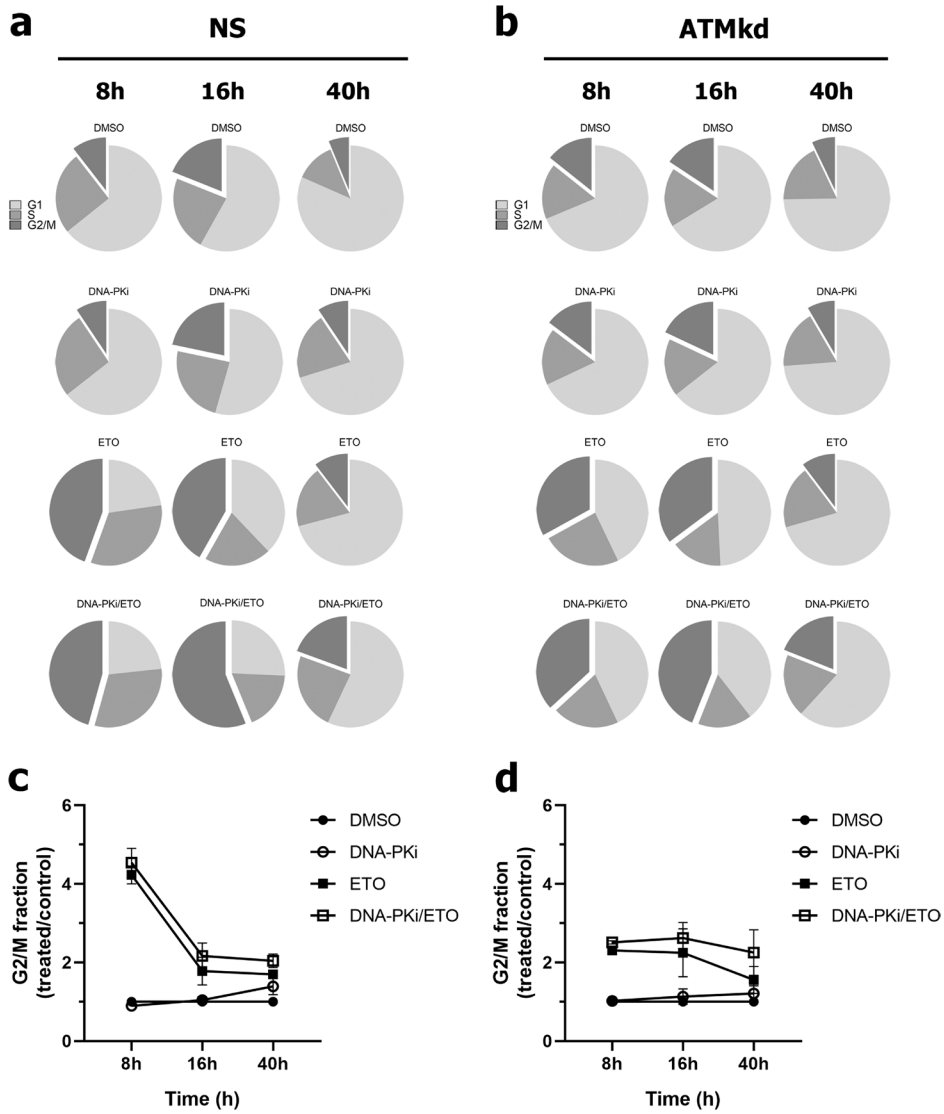

Fig. 4 Alterations of the cell cycle distributions after DNA-PKcs inhibition in ATM-proficient and -deficient cells treated with ETO. Pie graphs representation of the mean values for G1, S and G2 phases of the cell cycle in (**a**) HeLa NS and (**b**) HeLa ATM^{kd} cells at different time points. The G2/M fraction from treated versus control samples in (**c**) HeLa NS and (**d**) HeLa ATM^{kd} cells at 8, 16 and 40 h after treatment with ETO is represented

DNA-PKi/PARP-1i/ETO (0.19 ± 0.04) compared to DNA-PKi/ETO. In NS cells, it was observed an insignificant decrease in the values of dicentric chromosomes when treated with PARP-1i/ETO (0.21 ± 0.05) or DNA-PKi/PARP-1i/ETO (0.25 ± 0.05) in relation with DNA-PKi/ETO.

To assess persistent chromosome damage, the occurrence of chromatid- and chromosome-type aberrations was analyzed at 6 days (144 h) post-treatment. As shown in Figs. 5b and 5d, a significant increase in the formation of chromatid and chromosome breaks and exchanges was detected in NS cells following treatment with DNA-PKi/ETO compared to ETO alone. In addition, the increments were higher in HeLa ATM^{kd} cells. We observed substantially raised levels of acentric fragments (8.8-fold, Fig. 5b) and mainly, telomeric associations (16.4-fold, Fig. 5d) in ATM-deficient cells treated with DNA-PKi/ETO

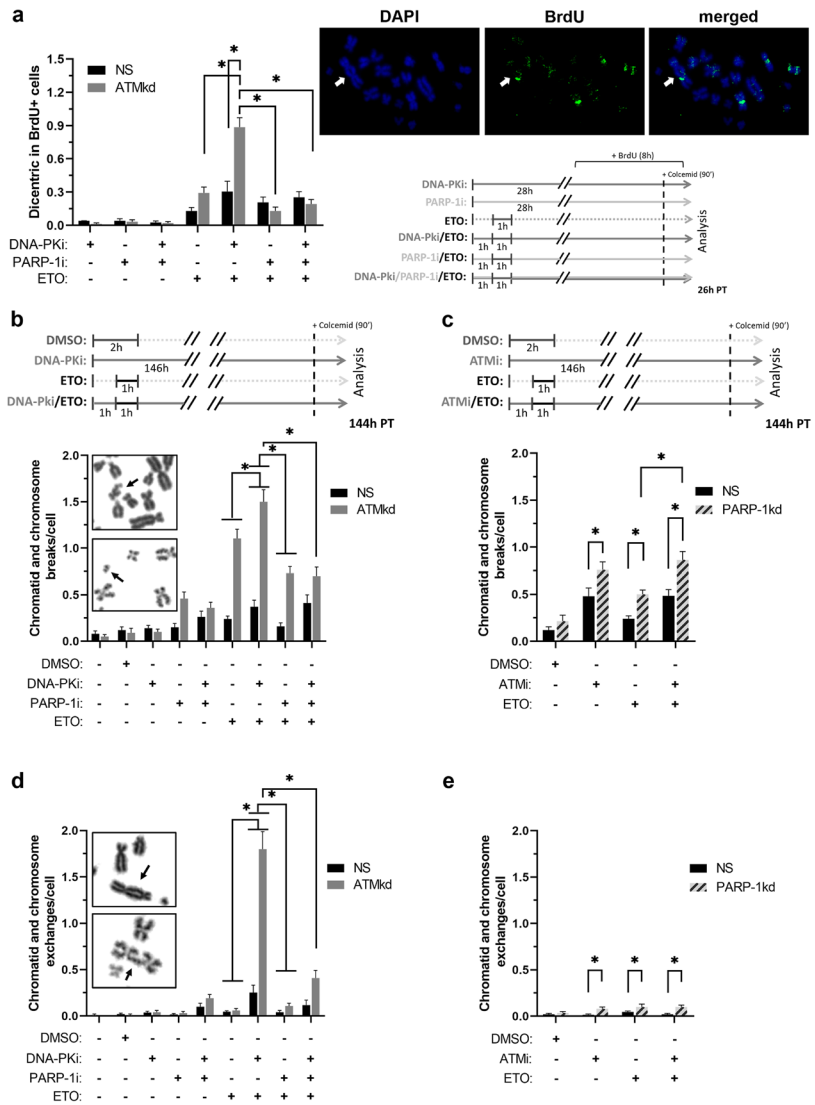

Fig. 5 Long-term structural chromosome aberrations induced by ETO in ATM-defective cells with impaired c-NHEJ or alt-EJ repair pathways. **a**. *Left panel:* Bar graph showing dicentric chromosomes in BrdU positive HeLa NS and ATM^{kd} cells at 26 h post-treatment (PT). *$p < 0.0001$. *Right upper panel:* Immunofluorescence images showing a metaphase spread with BrdU-incorporated chromosomes. *Right upper panel:* Immunofluorescence images showing metaphase chromosomes with BrdU incorporated. White arrow indicates dicentric chromosome. *Right lower panel:* Schematic representation of treatments over the time until the analysis. **b** and **d**. Chromatid- and chromosome-type aberrations in HeLa NS and ATM^{kd} cells following pre-treatment with DNA-PKi (NU7026 10 μM) or PARP-1i (BYK204165 10 μM) or both inhibitors and ETO treatment at 6 days (144 h) PT. **b.** *Upper panel:* Schematic representation of treatments (for b and d) over the time until analysis. Chromatid and chromosome breaks (**b**) and exchanges (**d**) were increased in HeLa ATM^{kd} cells following treatment with DNA-PKi/ETO vs. ETO (*$p < 0.047$; *$p < 0.034$, respectively). Reduction of chromatid and chromosome breaks **(b)** and exchanges **(d)** frequencies in HeLa ATM^{kd} cells following PARP-1i/ETO or PARP-1i/DNA-PKi/ETO compared to DNA-PKi/ETO treatments was observed (*$p < 0.0001$). **b.** *Upper photograph inside graph*: chromatid break; *lower photograph inside graph*: acentric fragment. **d.** *upper photograph inside graph*: dicentric chromosome; *lower photograph inside graph*: telomeric association. **c** and **e**. Chromatid- and chromosome-type aberrations in HeLa NS and PARP-1^{kd} cells following pre-treatment with ATM inhibitor (KU55933 10 μM) and ETO at 6 days (144 h) PT. **c**. *Upper panel:* Schematic representation of treatments (c and e) over the time until analysis. *Lower panel:* Chromatid and chromosome breaks/cells, *$p < 0.025$. **e**. Chromatid and chromosome exchange/cells, *$p < 0.035$.

respect to NS. Again, to corroborate the involvement of alt-EJ in the formation of these chromosomal rearrangements, both cells were treated with ETO in combination with PARP-1i or DNA-PKi/PARPR-1i. The results denoted an important reduction in chromatid and chromosome exchanges in HeLa ATM^{kd} cells treated with PARP-1i/ETO (0.11 ± 0.03) or DNA-PKi/PARP-1i/ETO (0.41 ± 0.08) compared to DNA-PKi/ETO (1.80 ± 0.19, Fig. 5d). A basal increase in both chromatid breaks and exchanges in the presence of the combination DNA-PKi/PARP-1i was also observed.

The data obtained with ATM-deficiency and the PARP-1 inhibition were also supported by the analysis of PARP-1^{kd} cells, which retained a residual PARP-1 mRNA expression of $6.2 \pm 3.6\%$ (shPARP-1#2, in Supplementary Fig. S1c) compared to NS. HeLa PARP-1^{kd} cells pre-treated with the ATMi, KU55933, showed significantly ($p = 0.003$) increased levels of ETO-induced chromatid and chromosome breaks (Fig. 5c) as compared to those PARP-1^{kd} cells with fully active ATM. Interestingly, a low frequency of chromatid and chromosome exchanges was also detected on PARP-1^{kd} cells pre-treated with ATMi (Fig. 5e). Therefore, the chemical inhibition or the genetic down regulation of PARP-1, suppressed ETO-induced chromosomal rearrangement formation in an ATM-deficient environment.

Together, ETO-induced exchange-type aberrations, such as dicentric chromosomes and telomeric fusions, highlight the involvement of the alt-EJ pathway in the joining of incorrect DSB ends in an ATM- and DNA-PKcs-deficient context.

Abolishment of c-NHEJ, more than alt-EJ, in ATM deficient cells results in hypersensitivity to ETO

To test the sensitivity of HeLa cells to increasing doses of ETO in a combined scenario of ATM and DNA-PKcs deficiency, clonogenic survival assay was performed (Fig. 6). Both ATM-proficient and -deficient cells were pre-treated or not with DNA-PKi and treated with different concentrations of ETO. As shown in Fig. 6a, the sensitivity to ETO was not altered in NS cells by the DNA-PKi. However, the lack of ATM activity led to an increased sensitivity to ETO, which was greatly augmented by the DNA-PKi. On the other hand, we assessed whether inhibition of alt-EJ can affect similarly the sensitivity to ETO in an ATM-deficient context. Thus, NS and ATM^{kd} cells were pre-treated or not with a PARP-1i before treatment with increasing doses of ETO. The results shown in Fig. 6b indicate a similar sensitivity to ETO of NS cells in the presence or absence of PARP-1i. As depicted in Fig. 6b, the alt-EJ inhibition in ATM^{kd} cells resulted in a slight increase in the sensitivity to ETO, but just at the higher dose.

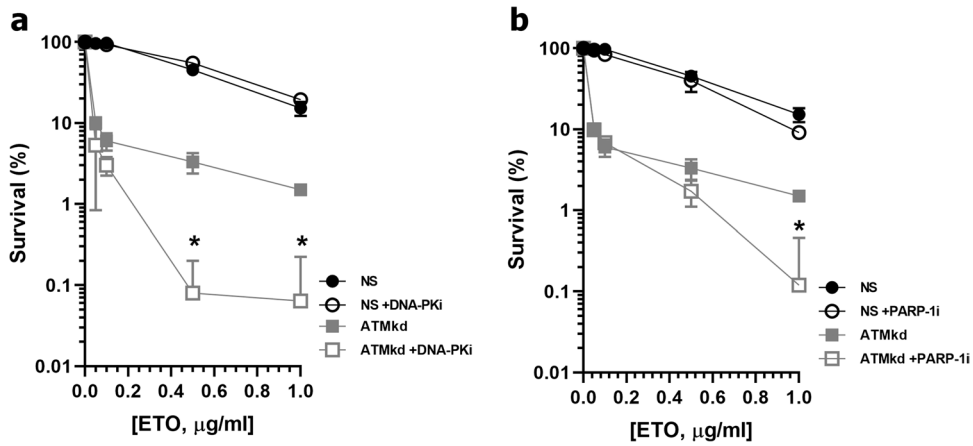

Fig. 6 Deficiency of ATM confers hypersensitivity to ETO in the presence of DNA-PKi or PARP-1i. **a**. Clonogenic survival assay of HeLa NS and ATM^{kd} cells in the presence or not of DNA-PKi (NU7026) for 2 h and different concentrations of ETO for 16 h. *p < 0.015. **b**. Clonogenic survival assay of HeLa NS and ATM^{kd} cells in the presence or not of PARP-1i (BYK204165) for 2 h and different concentrations of ETO for 16 h. *$p = 0.0076$

Together, our data demonstrate that lack of functional c-NHEJ in an ATM-deficient context results in hypersensitivity to ETO.

Discussion

ETO proved to be useful in the treatment of various human malignancies, including leukemia, lymphoma and solid tumors, but it is associated with the serious side effect of secondary leukemia resulting from the induction of chromosome translocations. This study was conducted to analyze the DNA-DSB repair mechanisms and the cellular progression of ETO-induced chromosomal damage in ATM-defective tumor cells with a non-oncogenic addiction to DNA-PKcs.

Both ATM and DNA-PKcs coordinate the DDR by phosphorylating hundreds of substrates to maintain the genome integrity (Blackford and Jackson 2017). ATM is central to the signal transduction process initiated by DSB. Defects in ATM underlie the autosomal recessive disorder A-T and cells from affected individuals are highly sensitive to radiation and radiomimetic drugs and present imperfect cell cycle checkpoint activation after exposure (Ambrose and Gatti 2013). In addition, mutation frequency analysis revealed that ATM is mutated in 5% of all cancers (Jette et al. 2020).

DNA-PKcs is also recruited to DSB by Ku, promoting c-NHEJ. C-NHEJ-deficient cells show proficient checkpoint activation, but fail to repair a large fraction of DSB. In human cells, c-NHEJ appears to repair nearly all DSB outside of S and G2 cell cycle phases, and even about 80% of DSB within S and G2, which are not proximal to a replication fork (Pannunzio et al. 2018).

Our results showed high percentages of γH2AX-positive cells following ETO and DNA-PKi/ETO treatments in G2 stage in both HeLa cell lines. This is in agreement with our previous findings in human normal and tumor cells (de Campos-Nebel, Larripa, and Gonzalez-Cid 2010; Palmitelli et al. 2015). In ATM^{kd} cells with DNA-PKcs inhibited, the phosphorylation of H2AX is likely to be mediated by the kinase activity of ATR [Blackford and Jackson, 2017].

It is widely accepted that unrepaired or misrepaired DSB lead to the formation of chromosome aberrations. Although the DSB induction was similar in both ATM-proficient and -deficient cells after DNA-PKi/ETO treatment, an excess of chromatid breaks was observed in the first metaphase of HeLa ATM^{kd} cells. This increase was also obtained in lymphocytes derived from the A-T patient compared to normal PBL.

Likewise, an increased frequency of unrepaired chromosome breaks in A-T human fibroblasts (Martin et al. 2003) and lymphoblastoid cells (Martin et al. 2009) was observed at the first metaphase after irradiation. Moreover, the large fraction of unrepaired DSB post-irradiation in A-T cells is thought to be the main responsible for radiosensitivity (Martin et al. 2009).

It was demonstrated that 10–20% of DSB, depending on the DNA damaging agent, requires the ATM activity for being repaired. These DSB correspond to damage occurring inside the heterochromatin, where ATM kinase activity is a prerequisite to open the chromatin structure, which allows the access of the repair machinery (Goodarzi et al. 2010). In addition, ATM was required for the efficient and accurate repair of Top2-blocked DSB induced by ETO in mice (Alvarez-Quilon et al. 2014).

The chromosome damage induced by ETO and DNA-PKcs inhibition in HeLa ATM^{kd} and A-T PBL was associated with a marked reduction in the number of analyzable metaphases. Hence, although most cells die in mitosis, a small number of them containing chromosomal alterations survive and continue to the following cell divisions.

To investigate the roles of ATM and DNA-PKcs in the regulation of HR, we monitored the RAD51 foci formation and the appearance of SCE following ETO treatment in G2 phase. Our findings support that ATM deficiency increases the RAD51 foci formation induced by ETO. Prior studies have shown an increased percentage of cells with RAD51 foci in human and mouse AT fibroblast cells exposed to ETO or irradiation, respectively (Yuan et al. 2003; Sun et al. 2010). In straight contrast, Beucher et al. (Beucher et al. 2009) and Bakr et al. (Bakr et al. 2015) reported that in response to irradiation, ATM deficiency compromised RAD51 foci formation and altered the efficiency of the HR process. It has been suggested that ATM could contribute to RAD51 turnover required for completion of HR (Shrivastav et al. 2009). Moreover, both RAD51 and RPA are polyubiquitinated by RFWD3 E3 ubiquitin ligase, favoring their degradation (Inano et al. 2017). This

degradation is regulated through phosphorylation of RFWD3 by ATR and ATM kinases. It is noteworthy that ATM knockdown might not be sufficient to inhibit the phosphorylation of RFWD3; and thus, favoring RAD51 accumulation.

We also found that ATM deficiency affected the SCE formation, showing lower levels than NS cells. Similarly, Bakr et al. (Bakr et al. 2015) reported that ATM was needed for the last steps in HR mechanism revealed by a reduced SCE rate in human cells treated with an ATMi before irradiation.

Since DNA-PKcs was reported to be a key regulator of both c-NHEJ and HR (Shrivastav et al. 2009), we also measured the HR repair of ETO-induced DSB in DNA-PKcs-inhibited cells. We observed a light increase of SCE frequencies respect to ETO alone in both cell lines. The reports referred to the effect of DNA-PKcs deficiency on HR repair events are controversial (Allen et al. 2002; Neal et al. 2011; Allen et al. 2003; Convery et al. 2005).

The focal accumulation of γH2AX in repair foci is a cytological manifestation of DSB formation, whose number associates linearly with the number of DNA breaks (Rothkamm and Lobrich 2003). The involvement of ATM and DNA-PKcs in the progression of DSB was assessed by counting γH2AX foci in the main nuclei of post-mitotic G1 phase cells. γH2AX foci were the result of persistent unrepaired or misrepaired events or recent DNA lesions generated during the previous mitosis. We detected that the lack of both activities caused an additive increase in the percentage of BN cells containing DSB, relative to either single factor. Both protein kinase activities were critical to guarantee genome integrity, whereas ATM deficiency led to an incomplete repair, DNA-PKcs inhibition resulted in an inaccurate repair, which in order stimulated the accumulation of chromosome breaks and rearrangements. Previous evidence showed that ATM and DNA-PKcs play complementary roles to allow a complete and legitimate DSB repair process (Martin et al. 2012).

In HeLa NS cells, the combined treatment DNA-PKi/ETO diminished the percentage of BN cells compared to ETO alone; however, in ATM^{kd} cells no difference between both treatments was detected. In this sense, the analyses of the cell cycle distribution showed that the G2/M fraction was not altered by the inhibition of DNA-PKcs in ETO-treated ATM^{kd} cells, in spite of the increased DNA damage found in BN cells.

Together with the evaluation of γH2AX, MRE11 foci formation was examined on matching samples in post-mitotic G1 cells. MRE11 is recruited to the DSB after damage, where it participates in DSB recognition, end-resection and repair (Lee et al. 2012). A direct relationship between cells containing γH2AX foci and cells with MRE11 labeling was found in ATM-deficient and -proficient HeLa cells during the different treatments.

The MRE11 foci formation in G1 phase suggests a contribution of the slow back-up and error prone alt-EJ repair pathway. When c-NHEJ is unable to repair DSB by the presence of a DNA-PKcs inhibitor, alt-EJ becomes the dominant pathway (Lobrich and Jeggo 2017). The increment of γH2AX-positive BN cells also suggested that an important subset of long-lived DSB in ATM-deficient cells might persist during several cell divisions.

The presence of rearrangements within the well-characterized breakpoint cluster region of the mixed lineage leukemia (MLL) gene on 11q23 is a hallmark of therapy-related leukemias following treatment with Top2 poisons (Zhang et al. 2021). The alt-EJ repair pathway operates with a speed and fidelity markedly lower than c-NHEJ and HR, causing elevated formation of chromosome translocations. Hence, although responsible for removing highly cytotoxic DNA ends from the genome, alt-EJ offers this function at the cost of increased translocation formation (Iliakis et al. 2015).

Furthermore, deficiencies in ATM and DNA-PKcs have been associated with elevated chromosome rearrangements and cancer predisposition (Bennardo and Stark 2010; Gunn et al. 2011). Taking together, we examined the possibility that alt-EJ might be involved in the repair of persistent DSB through the formation of dicentric chromosomes at second metaphase when ATM and DNA-PKcs were functionally compromised. Dicentric chromosomes and translocations occur with equal frequency and by identical mechanism (Yamauchi et al. 2011). The frequencies of dicentric chromosome were similar in NS treated with DNA-PKi/ETO and ATM^{kd} treated with ETO. However, ETO treatment in ATM-deficient cells with targeted inhibited DNA-PKcs caused a synergistic increase in the frequency of dicentric chromosomes compared to the

deficiency of individual activities. This is consistent with a previous report showing that ATM and DNA-PKcs can function in a common pathway to suppress ionizing radiation-induced dicentric chromosomes in normal human fibroblasts (Yamauchi et al. 2011). Thus, we considered that such increased frequency of dicentric chromosomes in ATM- and DNA-PKcs-deficient cells could reflect the contribution of alt-EJ pathway in the DSB repair.

To further examine the participation of alt-EJ in the repair of unresolved DSB, the occurrence of chromatid- and chromosome-type aberrations was analyzed at 6 days post-treatment. HeLa NS cells showed increased chromatid and chromosome breaks and exchanges after DNA-PKi/ETO treatment relative to ETO alone. However, ATM^{kd} cells showed a higher increase, and the chromosome aberrations after the combined treatment often included acentric fragments but mostly telomeric associations. Our results support a role of alt-EJ in the generation of genome instability in the absence of ATM and DNA-PKcs activities.

To gain more insight, NS and ATM^{kd} cells were treated with the PARP-1i. PARP-1 is an abundant nuclear enzyme of higher eukaryotes that recognizes DNA breaks and activates a MRE11-mediated DNA end resection of DSB to promote an alt-EJ repair mechanism (Caracciolo et al. 2021). PARP-1 also participates in multiple processes including chromatin remodeling, DNA replication fork progress, single- and double-strand break repair [Chaudhuri and Nussenzweig, 2017].

The results denoted a vast reduction in dicentric chromosomes and in chromatid and chromosome exchanges in ATM^{kd} cells treated with the combination PARP-1i/ETO or DNA-PKi/PARP-1i/ETO compared to DNA-PKi/ETO. These results were also corroborated with PARP-1^{kd} cells pre-treated with the ATMi, where the chromatid and chromosome exchange frequency induced by ETO was low. Indeed, either PARP-1 chemical inhibition or genetic knockdown decreased chromosomal rearrangement formation.

Regarding the exchange-type aberrations induced by ETO, we established that dicentric chromosomes and telomeric association in an ATM- and DNA-PKcs-deficient context emphasized the participation of alt-EJ pathway in the incorrect joining of DNA ends.

Bhargava et al. (Bhargava et al. 2020) described that the recognition of uncapped telomeres by ATM activates the end joining pathway responsible for end-to-end fusions between non-homologous chromosomes or sister chromatids that give rise to dicentric chromosomes. Dicentric chromosomes are highly unstable during mitosis, since they contain two centromeres attached to both spindle poles, being pulled in opposing directions during anaphase (Gascoigne and Cheeseman 2013). Therefore, both dicentric chromosomes and telomeric associations amplify genome instability by promoting the formation of chromosomal rearrangements through breakage-fusion-bridge cycles.

Next, we analyzed the sensitivity of HeLa cells to ETO in a combined scenario of ATM and DNA-PKcs or PARP-1 deficiencies. The sensitivity of NS cells to ETO was not altered by the presence of DNA-PKi or PARP-1i. In contrast, Willmore et al. (2004) reported an increased sensitivity of K562 cell line to ETO when combined with the DNA-PKi NU7026.

However, ATM^{kd} cells showed an important sensitivity to ETO, which was substantially increased by DNA-PKi, and to a lower extent, PARP-1i. The diminished clonogenic survival was related to the synergy between the lacks of functional c-NHEJ with the ATM deficiency.

Therefore, our results confirm a synthetic lethality phenotype between ATM and DNA-PKcs, and establish that both proteins are required for efficient and accurate repair of ETO-induced DSB in order to avoid genome instability. However, the findings of long-term alt-EJ mediated stable chromosome aberrations calls into question about the therapeutic strategy of targeting the non-oncogenic addiction to DNA-PKcs of ATM-defective tumors. In order to avoid cancer relapse, more complex combined therapies should be considered.

Acknowledgements This research was funded by Consejo Nacional de Investigaciones Científicas y Técnicas (CONICET) grant number PIP 0114/14; Agencia Nacional de Promoción Científica y Tecnológica (ANPCyT) grant number PICT 2015-3049; and Fundación A. J. Roemmers.

Author contributions [Marcelo de Campos Nebel], [Micaela Palmitelli] and [Marcela González-Cid] contributed to the study conception and design. Material preparation, data collection and analysis were performed by [Marcelo de Campos Nebel], [Micaela Palmitelli], [Josefina Pérez Maturo] and [Marcela González-Cid]. The first draft of the manuscript was

written by [Marcela González-Cid] and [Marcelo de Campos Nebel] and all authors commented on previous versions of the manuscript. All authors read and approved the final manuscript.

Declarations

Conflict of interest The authors declare no potential conflicts of interest.

References

Alhmoud JF, Woolley JF, Al Moustafa AE and Malki MI (2020) DNA damage/repair management in cancers. Cancers (Basel) 12:1050

Allen C, Kurimasa A, Brenneman MA, Chen DJ, Nickoloff JA (2002) DNA-dependent protein kinase suppresses double-strand break-induced and spontaneous homologous recombination. Proc Natl Acad Sci U S A 99:3758–3763

Allen C, Halbrook J, Nickoloff JA (2003) Interactive competition between homologous recombination and non-homologous end joining. Mol Cancer Res 1:913–920

Alvarez-Quilon A, Serrano-Benitez A, Lieberman JA, Quintero C, Sanchez-Gutierrez D, Escudero LM, Cortes-Ledesma F (2014) ATM specifically mediates repair of double-strand breaks with blocked DNA ends. Nat Commun 5:3347

Ambrose M, Gatti RA (2013) Pathogenesis of ataxia-telangiectasia: the next generation of ATM functions. Blood 121:4036–4045

Austen B, Skowronska A, Baker C, Powell JE, Gardiner A, Oscier D, Majid A, Dyer M, Siebert R, Taylor AM, Moss PA, Stankovic T (2007) Mutation status of the residual ATM allele is an important determinant of the cellular response to chemotherapy and survival in patients with chronic lymphocytic leukemia containing an 11q deletion. J Clin Oncol 25:5448–5457

Bakr A, Oing C, Kocher S, Borgmann K, Dornreiter I, Petersen C, Dikomey E, Mansour WY (2015) Involvement of ATM in homologous recombination after end resection and RAD51 nucleofilament formation. Nucleic Acids Res 43:3154–3166

Bennardo N, Stark JM (2010) ATM limits incorrect end utilization during non-homologous end joining of multiple chromosome breaks. PLoS Genet 6:e1001194

Beucher A, Birraux J, Tchouandong L, Barton O, Shibata A, Conrad S, Goodarzi AA, Krempler A, Jeggo PA, Lobrich M (2009) ATM and Artemis promote homologous recombination of radiation-induced DNA double-strand breaks in G2. EMBO J 28:3413–3427

Bhargava R, Fischer M, O'Sullivan RJ (2020) Genome rearrangements associated with aberrant telomere maintenance. Curr Opin Genet Dev 60:31–40

Blackford AN, Jackson SP (2017) ATM, ATR, and DNA-PK: The Trinity at the Heart of the DNA Damage Response. Mol Cell 66:801–17

de Campos-Nebel M, Larripa I and Gonzalez-Cid M (2010) 'Topoisomerase II-mediated DNA damage is differently repaired during the cell cycle by non-homologous end joining and homologous recombination', *PLoS One*, 5.

Caracciolo D, Riillo C, Di Martino MT, Tagliaferri P and Tassone P (2021) Alternative non-homologous end-joining: error-prone DNA repair as cancer's Achilles' heel. Cancers (Basel) 13:1392

Convery E, Shin EK, Ding Q, Wang W, Douglas P, Davis LS, Nickoloff JA, Lees-Miller SP, Meek K (2005) Inhibition of homologous recombination by variants of the catalytic subunit of the DNA-dependent protein kinase (DNA-PKcs). Proc Natl Acad Sci U S A 102:1345–1350

Deckbar D, Birraux J, Krempler A, Tchouandong L, Beucher A, Walker S, Stiff T, Jeggo P, Lobrich M (2007) Chromosome breakage after G2 checkpoint release. J Cell Biol 176:749–755

Del Nagro CJ, Choi J, Xiao Y, Rangell L, Mohan S, Pandita A, Zha J, Jackson PK, O'Brien T (2014) Chk1 inhibition in p53-deficient cell lines drives rapid chromosome fragmentation followed by caspase-independent cell death. Cell Cycle 13:303–314

Gascoigne KE, Cheeseman IM (2013) Induced dicentric chromosome formation promotes genomic rearrangements and tumorigenesis. Chromosome Res 21:407–418

Goodarzi AA, Jeggo P, Lobrich M (2010) The influence of heterochromatin on DNA double strand break repair: Getting the strong, silent type to relax. DNA Repair (amst) 9:1273–1282

Gunn A, Bennardo N, Cheng A, Stark JM (2011) "Correct end use during end joining of multiple chromosomal double strand breaks is influenced by repair protein RAD50 DNA-Dependent Protein Kinase DNA-PKcs, and Transcription Context." J Biol Chem 286:42470–42482

Iliakis G, Murmann T, Soni A (2015) Alternative end-joining repair pathways are the ultimate backup for abrogated classical non-homologous end-joining and homologous recombination repair: Implications for the formation of chromosome translocations. Mutat Res Genet Toxicol Environ Mutagen 793:166–175

Inano S, Sato K, Katsuki Y, Kobayashi W, Tanaka H, Nakajima K, Nakada S, Miyoshi H, Knies K, Takaori-Kondo A, Schindler D, Ishiai M, Kurumizaka H, Takata M (2017) RFWD3-Mediated Ubiquitination Promotes Timely Removal of Both RPA and RAD51 from DNA Damage Sites to Facilitate Homologous Recombination. Mol Cell 66(622–34):e8

Jeggo PA, Lobrich M (2006) Contribution of DNA repair and cell cycle checkpoint arrest to the maintenance of genomic stability. DNA Repair (amst) 5:1192–1198

Jette NR, Kumar M, Radhamani S, Arthur G, Goutam S, Yip S, Kolinsky M, Williams GJ, Bose P, Lees-Miller SP (2020) ATM-deficient cancers provide new opportunities for precision oncology. Cancers (Basel) 12:687

Jiang H, Reinhardt HC, Bartkova J, Tommiska J, Blomqvist C, Nevanlinna H, Bartek J, Yaffe MB, Hemann MT (2009) The combined status of ATM and p53 link tumor development with therapeutic response. Genes Dev 23:1895–1909

Kopp B, Khoury L, Audebert M (2019) Validation of the gammaH2AX biomarker for genotoxicity assessment: a review. Arch Toxicol 93:2103–2114

Lee KC, Padget K, Curtis H, Cowell IG, Moiani D, Sondka Z, Morris NJ, Jackson GH, Cockell SJ, Tainer JA, Austin CA (2012) MRE11 facilitates the removal of human

topoisomerase II complexes from genomic DNA. Biol Open 1:863–873
Lobrich M, Jeggo P (2017) A Process of Resection-Dependent Nonhomologous End Joining Involving the Goddess Artemis. Trends Biochem Sci 42:690–701
Martin M, Genesca A, Latre L, Ribas M, Miro R, Egozcue J, Tusell L (2003) Radiation-induced chromosome breaks in ataxia-telangiectasia cells remain open. Int J Radiat Biol 79:203–210
Martin M, Terradas M, Iliakis G, Tusell L, Genesca A (2009) Breaks invisible to the DNA damage response machinery accumulate in ATM-deficient cells. Genes Chromosomes Cancer 48:745–759
Martin M, Terradas M, Tusell L, Genesca A (2012) ATM and DNA-PKcs make a complementary couple in DNA double strand break repair. Mutat Res Rev Mutat Res 751:29–35
Meyer KN, Kjeldsen E, Straub T, Knudsen BR, Hickson ID, Kikuchi A, Kreipe H, Boege F (1997) Cell cycle-coupled relocation of types I and II topoisomerases and modulation of catalytic enzyme activities. J Cell Biol 136:775–788
Mladenov E, Magin S, Soni A, Iliakis G (2016) DNA double-strand-break repair in higher eukaryotes and its role in genomic instability and cancer: Cell cycle and proliferation-dependent regulation. Semin Cancer Biol 37–38:51–64
Neal JA, Dang V, Douglas P, Wold MS, Lees-Miller SP, Meek K (2011) Inhibition of homologous recombination by DNA-dependent protein kinase requires kinase activity, is titratable, and is modulated by autophosphorylation. Mol Cell Biol 31:1719–1733
Nitiss JL (2009) Targeting DNA topoisomerase II in cancer chemotherapy. Nat Rev Cancer 9:338–350
Obe G, Durante M (2010) DNA double strand breaks and chromosomal aberrations. Cytogenet Genome Res 128:8–16
Palmitelli M, de Campos-Nebel M, Gonzalez-Cid M (2015) Progression of chromosomal damage induced by etoposide in G2 phase in a DNA-PKcs-deficient context. Chromosome Res 23:719–732
Pannunzio NR, Watanabe G, Lieber MR (2018) Nonhomologous DNA end-joining for repair of DNA double-strand breaks. J Biol Chem 293:10512–10523
Perez Maturo J, Gonzalez Cid M, Zavala L, Rodriguez Quiroga S, Kauffman MA (2020) Novel Variants in ATM Causing Mild Ataxia-Telangiectasia: From Benchside to Bedside and Back Again. Mov Disord Clin Pract 7:727–729
Ranjha L, Howard SM, Cejka P (2018) Main steps in DNA double-strand break repair: an introduction to homologous recombination and related processes. Chromosoma 127:187–214
Riabinska A, Daheim M, Herter-Sprie GS, Winkler J, Fritz C, Hallek M, Thomas RK, Kreuzer KA, Frenzel LP, Monfared P, Martins-Boucas J, Chen S, Reinhardt HC (2013) Therapeutic targeting of a robust non-oncogene addiction to PRKDC in ATM-defective tumors. Sci Transl Med 5:189ra78
Rothkamm K, Lobrich M (2003) Evidence for a lack of DNA double-strand break repair in human cells exposed to very low x-ray doses. Proc Natl Acad Sci U S A 100:5057–5062
Roukos V, Misteli T (2014) The biogenesis of chromosome translocations. Nat Cell Biol 16:293–300
Seol JH, Shim EY, Lee SE (2018) Microhomology-mediated end joining: Good, bad and ugly. Mutat Res 809:81–87
Shiloh Y, Ziv Y (2013) The ATM protein kinase: regulating the cellular response to genotoxic stress, and more. Nat Rev Mol Cell Biol 14:197–210
Shrivastav M, Miller CA, De Haro LP, Durant ST, Chen BP, Chen DJ, Nickoloff JA (2009) DNA-PKcs and ATM co-regulate DNA double-strand break repair. DNA Repair (amst) 8:920–929
Sonoda E, Sasaki MS, Morrison C, Yamaguchi-Iwai Y, Takata M, Takeda S (1999) Sister chromatid exchanges are mediated by homologous recombination in vertebrate cells. Mol Cell Biol 19:5166–5169
Sun J, Oma Y, Harata M, Kono K, Shima H, Kinomura A, Ikura T, Suzuki H, Mizutani S, Kanaar R, Tashiro S (2010) ATM modulates the loading of recombination proteins onto a chromosomal translocation breakpoint hotspot. PLoS ONE 5:e13554
Willmore E, de Caux S, Sunter NJ, Tilby MJ, Jackson GH, Austin CA, Durkacz BW (2004) A novel DNA-dependent protein kinase inhibitor, NU7026, potentiates the cytotoxicity of topoisomerase II poisons used in the treatment of leukemia. Blood 103:4659–4665
Yamauchi M, Suzuki K, Oka Y, Suzuki M, Kondo H, Yamashita S (2011) Mode of ATM-dependent suppression of chromosome translocation. Biochem Biophys Res Commun 416:111–118
Yuan SS, Chang HL, Lee EY (2003) Ionizing radiation-induced Rad51 nuclear focus formation is cell cycle-regulated and defective in both ATM(-/-) and c-Abl(-/-) cells. Mutat Res 525:85–92
Zhang W, Gou P, Dupret JM, Chomienne C, Rodrigues-Lima F (2021) Etoposide, an anticancer drug involved in therapy-related secondary leukemia: Enzymes at play. Transl Oncol 14:101169